Rend. Lincei Mat. Appl. 28 (2017), 777–805
DOI 10.4171/RLM/785

Partial Differential Equations — *Towards a gradient flow for microstructure*, by Patrick Bardsley, Katayun Barmak, Eva Eggeling, Yekaterina Epshteyn, David Kinderlehrer and Shlomo Ta'asan, communicated on June 15, 2017.

Dedicated to the memory and enduring legacy of Professor Ennio De Giorgi.

Abstract. — A central problem of microstructure is to develop technologies capable of producing an arrangement, or ordering, of a polycrystalline material, in terms of mesoscopic parameters, like geometry and crystallography, appropriate for a given application. Is there such an order in the first place? Our goal is to describe the emergence of the grain boundary character distribution (GBCD), a statistic that details texture evolution discovered recently, and to illustrate why it should be considered a material property. For the GBCD statistic, we have developed a theory that relies on mass transport and entropy. The focus of this paper is its identification as a gradient flow in the sense of De Giorgi, as illustrated by Ambrosio, Gigli, and Savaré. In this way, the empirical texture statistic is revealed as a solution of a Fokker–Planck type equation whose evolution is determined by weak topology kinetics and whose limit behavior is a Boltzmann distribution. The identification as a gradient flow by our method is tantamount to exhibiting the harvested statistic as the iterates in a JKO implicit scheme. This requires several new ideas. The development exposes the question of how to understand the circumstances under which a harvested empirical statistic is a property of the underlying process.

Key words: Coarsening, texture development, large metastable networks, critical event model, entropy-based theory, free energy, Fokker–Planck equation, Kantorovich–Rubinstein–Wasserstein metric

Mathematics Subject Classification: 37M05, 35Q80, 93E03, 60J60, 35K15, 35A15

1. Introduction

Cellular networks are ubiquitous in nature. They exhibit behavior on many different length and time scales and are generally metastable. Most technologically useful materials are polycrystalline microstructures composed of a myriad of small monocrystalline grains separated by grain boundaries, and thus comprise cellular networks. The energetics and connectivity of the grain boundary network plays a crucial role in determining the properties of a material across a wide range of scales. A central problem is to develop technologies capable of producing an arrangement of grains that provides for a desired set of material properties. The traditional focus has been on distributions of geometric features, like cell size, and a preferred distribution of grain orientations, termed texture.

Attaining these gives the configuration order in a statistical sense. More recent mesoscale experiment and simulation permit harvesting large amounts of information about both geometric features and crystallography of the boundary network in material microstructures, [2, 3, 19, 25, 26]. This has led us to the notion of the Grain Boundary Character Distribution. The GBCD is an empirical distribution of the relative length (in 2D) or area (in 3D) of interface with a given lattice misorientation and grain boundary normal. It is a leading candidate to characterize texture of the boundary network.

For the GBCD statistic, we develop a theory that relies on mass transport and entropy. A consequence now is that we seek to identify it as a gradient flow in the sense of De Giorgi as developed by Ambrosio, Gigli, and Savaré, [4, 5]. In this way, the empirical texture statistic is revealed as a solution of a Fokker–Planck type equation whose evolution is determined by weak topology kinetics and whose limit behavior is the observed Boltzmann distribution for the prescribed interfacial energy density. To achieve this we must determine first an appropriate dissipation relation, for which we introduce the discrete iteration principle first noted in [18]. Further viewing the GBCD as samples of a process motivates us to adjust the time scale in a nontrivial manner, precisely matching the evolution of a Fokker Planck Equation. That the simulation time scale must be coordinated to the physical time scale is a challenging yet persistent problem. It arises even in the simulation of the simplest systems, like the Ehrenfest Urn. This identification as a gradient flow is tantamount to exhibiting the harvested statistic as the iterates in a JKO implicit scheme, [18]. Enroute to the GBCD results, we also study a simpler 1D model coarsening system that shares many qualitative features with the GBCD. The development exposes the question of how to understand the circumstances under which a harvested empirical statistic is a property of the underlying process.

The GBCD viewpoint on texture and texture dependent properties is an active area of materials research [1, 16]. Viewing the evolution of complex systems as gradient flows is also discussed in the very interesting work [23].

2. Recapitulation of mesoscale theory and 2D computational model: the coarsening network

Let us briefly review a mesoscale theory of microstructural evolution and a 2D computational model based on this theory; see [7–11, 13] for a more detailed discussion and [12] for a discussion directed to materials researchers. Coarsening occurs when growth, namely evolution of cells and cell boundaries, occurs in a confined space. There is a common denominator theory for the mesoscale description of microstructural evolution. This is growth by curvature, the Mullins Equation (2) below, for the evolution of curves or arcs individually or in a network. Boundary conditions must be imposed where the arcs meet to have a well-posed system. We consider the Herring Condition, (3), which is the natural boundary condition at equilibrium for the Mullins Equation. Let α denote the misorientation between two grains separated by an arc Γ, as shown in Figure 1,

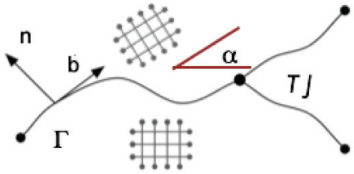

Figure 1. An arc Γ with normal n, tangent t, and lattice misorientation α, illustrating lattice elements.

with normal $n = (\cos\theta, \sin\theta)$, tangent direction b and curvature κ. Let $\psi = \psi(\theta, \alpha)$ denote the interfacial energy density on Γ. So

$$\Gamma : x = \xi(s,t), \quad 0 \leqq s \leqq L,\ t > 0, \tag{1}$$

with

$$b = \frac{\partial \xi}{\partial s} \text{ (tangent)} \quad \text{and} \quad n = Rb \text{ (normal)}$$

$$v = \frac{\partial \xi}{\partial t} \text{ (velocity)} \quad \text{and} \quad v_n = v \cdot n \text{ (normal velocity)}$$

where R is a positive rotation of $\pi/2$. The Mullins Equation of evolution for the curves or arcs is

$$v_n = (\psi_{\theta\theta} + \psi)\kappa \quad \text{on } \Gamma. \tag{2}$$

In our model, we assume that only triple junctions are stable and that the Herring Condition holds at triple junctions. This means that whenever three curves $\{\Gamma^{(1)}, \Gamma^{(2)}, \Gamma^{(3)}\}$, meet at a point p the force balance, holds:

$$\sum_{i=1,\ldots,3} (\psi_\theta n^{(i)} + \psi b^{(i)}) = 0. \tag{3}$$

The energy of Γ is $\int_\Gamma \psi|b|\,ds$ and it is easy to verify that the instantaneous rate of change of this energy is

$$\frac{d}{dt}\int_\Gamma \psi|b|\,ds = -\int_\Gamma v_n^2\,ds + v \cdot (\psi_\theta n + \psi b)|_{\partial\Gamma} \tag{4}$$

Let us consider now a planar network of grains bounded by $\{\Gamma_i\}$ subject to some condition at the border of the region they occupy, like fixed end points or periodicity, cf. Figure 2. The total energy of the system is defined as

$$E(t) = \sum_{\{\Gamma_i\}} \int_{\Gamma_i} \psi|b|\,ds \tag{5}$$

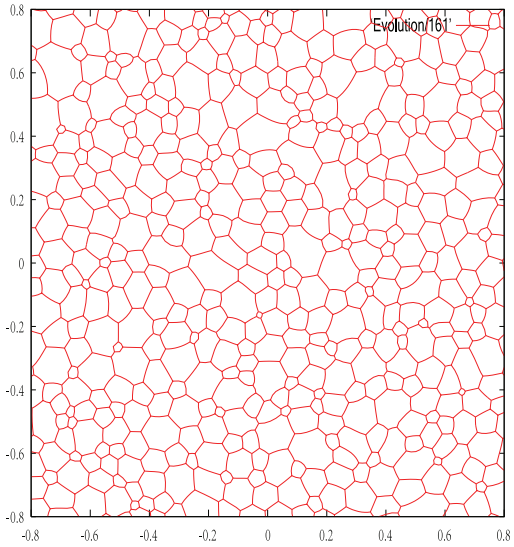

Figure 2. Example of a cellular network from simulation. This is from a small simulation with constant energy density and periodic conditions at the border of the configuration [9].

Therefore, due to the Herring Condition (3), the instantaneous rate of change of the energy

$$\frac{d}{dt}E(t) = -\sum_{\{\Gamma_i\}}\int_{\Gamma_i} v_n^2\,ds + \sum_{TJ} v\cdot\sum(\psi_\theta n + \psi b) \tag{6}$$

$$= -\sum_{\{\Gamma_i\}}\int_{\Gamma_i} v_n^2\,ds$$

$$\leqq 0,$$

Hence, in an interval $(t_0, t_0+\tau)$ where there are no critical or rearrangement events (grain deletion and facet interchange), we may integrate (6) to obtain a local dissipation equation for the grain boundary network

$$\sum_{\{\Gamma_i\}}\int_{t_0}^{t_0+\tau}\int_{\Gamma_i} v_n^2\,ds\,dt + E(t_0+\tau) = E(t_0) \tag{7}$$

which has a strong resemblance to the simple dissipation relation for an ensemble of inertia free springs with friction. Next, assume for simplicity, that the energy density is independent of the normal direction, so $\psi = \psi(\alpha)$. Then (2) and (3) become

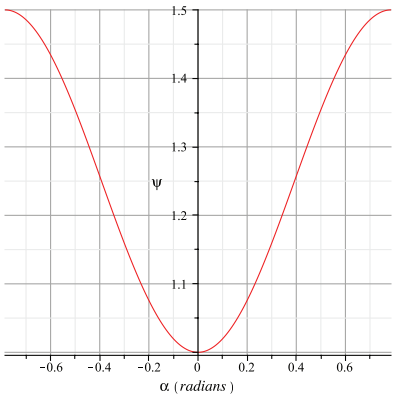

Figure 3. The energy density $\psi(\alpha) = 1 + \varepsilon \sin^2 2\alpha$, $\varepsilon = \frac{1}{2}$, used for the examples of coarsening in cellular systems in this note.

$$v_n = \psi\kappa \quad \text{on } \Gamma \tag{8}$$

$$\sum_{i=1,\ldots,3} \psi b^{(i)} = 0 \quad \text{at } p, \tag{9}$$

where p denotes a triple junction. For this situation one can define the Grain Boundary Character Distribution, GBCD,

$$\rho(\alpha, t) = \text{relative length of arc of misorientation } \alpha \text{ at time } t, \tag{10}$$

$$\text{normalized so that } \int_\Omega \rho \, d\alpha = 1.$$

Evolution of GBCD statistics will be the focus of our study below.

The 2D computational model is based on first initializing a configuration of cells and their boundary arcs, usually by a modified Voronoi tessellation, and numerically solving the system of Mullins evolution equation (2) for the network of curves/grain boundaries subject to the boundary conditions at the triple junctions (3) while managing the critical events. This computational model must be designed so it is robust and so reliable statistics can be harvested. Owing to the size and complexity of the 2D grain boundary network there are number of challenges in designing the method. These include

- dynamic management of the data structure of cells, facets, and triple junctions
- management of the computational domain
- initialization of the computation
- resolving the equations (2) with sufficient accuracy while
- maintaining the triple junction boundary condition (3)

Furthermore, it is important to identify some reliable diagnostics/measures to understand the accuracy of the 2D model and resulting large scale simulations.

For example, it is known that the average area of cells grows linearly even in very casual simulations of coarsening, although more careful diagnostics show that the Herring Condition (3) may fail if it is not resolved with sufficient accuracy. As noted in the introduction, this will lead to an unreliable determination of the GBCD.

In view of the dissipation inequality (6) the evolution of the grain boundary system may be viewed as a modified steepest descent for the energy. Therefore, the cornerstone of our 2D computational model, which assures its stability, is the discrete dissipation inequality for the total grain boundary energy which holds when the discrete Herring Condition is satisfied. In general, a discrete dissipation principle ensures the stability and convergence of numerical schemes to the continuous solution. Here we work with a weak formulation, a variational principle, to avoid the additional complexity of higher order spaces. It is not necessary to know the normal direction, nor is there explicit use of curvature.

What follows is a more detailed explanation of the simulation procedure. First, we initialize a configuration of cells and their boundary arcs, by a Voronoi diagram with N_0 seeds place randomly in the computational domain and we impose 'periodic boundary conditions' on the border of the computational domain. We would like to emphasize that we do not work with functions which have periodic boundary conditions but with cell structures which mirror each other near the borders of the computational domain and they must be dynamically updated. This is an important part of the algorithm and it is necessary in order that the statistics always sample in the same computational domain.

Each cell is assigned an orientation and the misorientation parameter of a boundary is the difference of the orientations of the grains which share it. Typically the orientations are normally distributed, so the misorientations are also normally distributed.

The simulation of the planar grain boundary network proceeds in three principal steps by evolving first the grain boundaries, according to a modified steepest descent (Mullins Equation), and then updating the triple points according to the Herring Condition (3), imposed at the triple junctions, and finally managing the rearrangement events in a way that preserves (6). In our 2D computational model, grain boundaries are defined by the set of nodal points and are approximated using linear elements. In the algorithm, we define a global mesh size, h, and uniformly discretized grain boundaries with local mesh size (distance between neighboring nodal points) which depends on h. Due to the frequency of critical events, we have used a first order method in time, namely the Forward Euler method. Increasing the order of time discretization to 2 by using a predictor corrector method did not affect the distribution functions, which is the focus of this study.

Resolution of the Herring Condition: To satisfy the Herring Condition (3) one has to solve the nonlinear equation to determine the new position of the triple junction [20]. We use a Newton's method with line search [17] to approximate the new position for the triple junction. As the initial guess for Newton's method, we determine the position of the triple point by defining the velocity of the triple

junction to be proportional to the total line stress at that point with coefficient of the proportionality equal to the mobility. This is also dissipative for the network. The Newton algorithm stops if it exceeds a certain tolerance on the number of the iterations. If the Newton's algorithm converges, the Herring Condition (3) is satisfied with the machine precision accuracy at the new position of the triple junction. If Newton's algorithm fails to converge at some triple junctions (this happens when we work with very small cells) we use our initial guess to update its position.

Critical events: As grain growth proceeds, critical events occur. When grain boundaries (GB) shrink below a certain size, they trigger one or more of the following processes (i) short GB removal, (ii) splitting of unstable junctions (where more then three GB meet) (ii) fixing double GB (GB that share two vertices).

Removal of short GB: A short GB whose length is decreasing is removed. If its length is increasing, it is not removed.

Splitting unstable vertices: When a GB disappears, new vertices may appear where more than three edges meet. These are unstable and split, introducing a new vertex and a new GB of short length, reducing the number of edges meeting at the unstable junctions. This process continues until all vertices are triple junctions. Details of each split are designed to maximally decrease the energy.

3. Theory of the GBCD

The issue we address now is the nature of the evolution of the GBCD. From (5) it is easy to justify an energy

$$\int_{\Omega} \psi \rho \, d\alpha$$

and a kinetic term that needs to be allied to (6). In addition the ensemble has been upscaled in an irreversible fashion, necessitating the introduction of an entropic contribution. This upscaling passes from a mesoscale process of the evolution of individual arcs to the evolution of a harvested statistic. Formally it is analogous to the elementary calculation, due to Boltzmann himself, of the emergence of the free energy associated to occupation numbers of bins from the individual particles in the bins. Equally appropriate is the Ehrenfest Urn, where the microscopic process of moving particles between urns is 'upscaled' to the mesoscopic Ornstein–Uhlenbeck process of the occupation of the urns. These are standard statistical physics considerations.

To place this in perspective, we briefly discuss critical events or rearrangement events. For an individual cell in an ensemble with constant facet energy density, evolution laws (2) and (3) lead to the well known von Neumann–Mullins $n-6$ rule, [28], [24]: the rate of change of area of an n-faceted cell with constant surface energy density and exterior angles meeting at $2\pi/3$ is proportional to $n-6$,

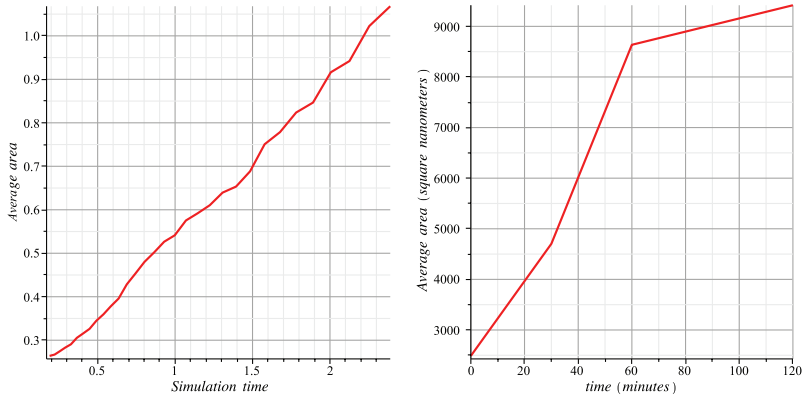

Figure 4. (a) Simulations tend to exhibit linear average growth in area. Shown is average area of the five sided facet class in a typical simulation (arbitrary units). (b) Average area in nm^2 of five sided grains in an Al columnar grain structure increases (time in minutes).

that is,

$$\frac{dA_n}{dt} = c(n-6), \quad \text{where } A_n \text{ is the area of an } n\text{-faceted cell} \tag{11}$$

and $c > 0$ is some material constant. The $2\pi/3$ angle is just (3) when the surface energy density is constant.

One can see from Figure 4 that, contrary to (11), the average area of five sided grains during simulation or a growth experiment, in this case on an Al thin film, increase several-fold during coarsening. The Von Neumann–Mullins $n-6$ rule (11) does not fail, but most of the 5-faceted cells observed at a chosen time t are descendants of cells with $6, 7, 8, \ldots$ facets at some time earlier than t. Thus in the network setting, the topological changes play a crucial role. Simulations are generally stopped when 80% of initial cells have been deleted; they stagnate at about this level. Although small cells with small numbers of facets will eventually be deleted from the system, their effect on the configuration is essentially random.

We shall consider the standard configurational entropy,

$$+\sigma \int_\Omega \rho \log \rho \, d\alpha, \tag{12}$$

although this is not the only choice. Determining the 'temperature' parameter σ will be discussed later. Minimizing (12) favors the uniform state, which would be the situation were $\psi(\alpha) = \text{constant}$. A tantalizing clue to the development of texture will be whether or not this entropy strays from its minimum during the simulation.

Here we shall be aided by a simplified 1D critical event model that was considered in [7–11, 13] to develop the mathematical theory for the GBCD. This simplified 1D network has a strong similarity to the 2D network discussed in Sec-

tion 2, including its gradient flow character. Its analysis is more accessible owing to a kinetic term that leads more directly to a mass transport interpretation.

In this simplified model, the cells are intervals on a line segment in 1D. Each cell represents a "grain boundary," but not the grain, with a given misorientation parameter subject to nearest neighbor interactions. Thus, consider a partition of a circle of circumference $L > 0$ by N randomly chosen points, equivalently a partition of the interval $[0, L] \subset \mathbb{R}$ by points x_i, $i = 1 \dots N$, where $x_i < x_{i+1}$, $i = 1 \dots N-1$ and x_{N+1} identified with x_1. For each interval/grain boundary $[x_i, x_{i+1}]$, $i = 1 \dots, N$ select a random misorientation parameter $\alpha_i \in \mathbb{R}$. The intervals $[x_i, x_{i+1}]$ correspond to grain boundaries and the points x_i represent the triple junctions. Select an energy density function $\psi(\alpha)$ and define the energy of the 1D grain boundary network

$$E = \sum_{i=1 \dots N} \psi(\alpha_i)(x_{i+1} - x_i). \tag{13}$$

Gradient flow kinetics are imposed with respect to (13), which is just the system of ordinary differential equations

$$\frac{dx_i}{dt} = \psi(\alpha_i) - \psi(\alpha_{i-1}), \quad i = 2 \dots N, \quad \text{and} \quad \frac{dx_1}{dt} = \psi(\alpha_1) - \psi(\alpha_N). \tag{14}$$

We also define the velocity v_i of the i^{th} boundary as

$$v_i = \frac{dx_{i+1}}{dt} - \frac{dx_i}{dt} = \psi(\alpha_{i-1}) - 2\psi(\alpha_i) + \psi(\alpha_{i+1}). \tag{15}$$

The grain boundary velocities are constant until one of the boundaries collapses. That segment is removed from the list of current grain boundaries and the velocities of its two neighbors are changed due to the emergence of a new junction. Each such deletion event rearranges the network and, thus, affects its subsequent evolution just as in the 2D cellular network.

Similar to the dissipation principle (6) of the 2D grain boundary network, there is an analogous dissipation inequality for the 1D network of grain boundaries. At any time t between deletion events,

$$\frac{dE}{dt} = -\sum \frac{dx_i^2}{dt} \leqq 0. \tag{16}$$

Hence, similar to (7), one can show dissipation equality and inequality,

$$\int_{t_0}^{t_0+\tau} \frac{dx_i^2}{dt}\, dt + E(t_0 + \tau) = E(t_0), \tag{17}$$

and expressing the first term in (17) in terms of grain boundary velocity (15), we obtain a dissipation inequality of the form:

$$\int_{t_0}^{t_0+\tau} \frac{1}{4} \sum_{i=1}^{n} v_i^2(t)\, dt + E(t_0 + \tau) \leqq E(t_0). \tag{18}$$

The grain growth analog (18) of the spring-mass-dashpot-like local dissipation equality is valid under assumption that there are no critical events in a time interval $(t_0, t_0 + \tau)$, $\tau > 0$ is sufficiently small.

Similar to the 2D model in Section 2, a GBCD for the simplified 1D network can be introduced [7–11, 13]. Consider a new ensemble based on the misorientation parameter α where we take $\Omega : -\frac{\pi}{4} \leqq \alpha \leqq \frac{\pi}{4}$, (in order to compare with the two dimensional network for which we are imposing "cubic" symmetry, i.e., "square" symmetry in the plane). The GBCD, or the character distribution in this context, is the histogram $\rho(\alpha, t)$ of lengths of intervals sorted by misorientation α scaled to be a probability distribution on Ω, so in particular, the statistic satisfies

$$\int_\Omega \rho(\alpha, t)\, d\alpha = 1.$$

Now, using the energy of the network (13), one may express local dissipation inequality (18) in terms of character distribution

$$\mu_0 \int_{t_0}^{t_0+\tau} \int_\Omega \left|\frac{\partial \rho}{\partial t}\right|^2 d\alpha\, dt + \int_\Omega \rho\psi\, d\alpha|_{t_0+\tau} \leqq \int_\Omega \rho\psi\, d\alpha|_{t_0}, \tag{19}$$

where μ_0 is some positive constant, [7–11, 13]. As it was mentioned above, the local dissipation inequality (18) or equivalently the dissipation inequality (19) is valid under the assumption that there are no critical events in the system. To complete the energetic description of the system, incorporating the effects of critical events into the system, we introduce a free energy defined as

$$F_\sigma(\rho) = \int_\Omega (\rho\psi + \sigma\rho \log \rho)\, d\alpha. \tag{20}$$

The diffusion-like parameter σ will be determined later.

The details of how we address the kinetic term in (19) are found in [7–11, 13] and only the conclusion is quoted here. Under some assumptions we find that

$$\int_\Omega v^2 \rho\, d\alpha \leqq C_1 \int_\Omega \left|\frac{\partial \rho}{\partial t}\right|^2 d\alpha, \tag{21}$$

where the pair (v, ρ) satisfy the continuity equation

$$\rho_t + (v\rho)_\alpha = 0, \quad \text{in } \Omega,\ t > 0. \tag{22}$$

In this way we extend (19) to a proposed dissipation relation for the GBCD

$$\mu_1 \int_{t_0}^{t_0+\tau} \int_\Omega v^2 \rho\, d\alpha\, dt + F_\sigma(\rho)|_{t_0+\tau} \leqq F_\sigma(\rho)|_{t_0} \tag{23}$$

In general, the (Kantorovich–Rubinstein–)Wasserstein distance $d(\rho, \rho^*)$ between ρ, ρ^*, two probability measures, is given by

$$d(\rho,\rho^*)^2 = \int_\Omega (x-\phi(x))^2\rho\,dx, \text{ where} \tag{24}$$

ϕ is the transfer function from ρ to ρ^*.

It is well known that it is given by the Benamou–Brenier formula

$$\frac{1}{\tau}d(\rho,\rho^*)^2 = \inf_{(v,\rho)}\int_0^\tau\int_\Omega v^2\rho\,dx\,dt \text{ subject to} \tag{25}$$

$$\rho_t + (v\rho)_x = 0, \quad \text{in } \Omega,\ 0<t<\tau,\ \rho|_{t=0}=\rho^*,\ \rho|_{t=\tau}=\rho.$$

Finally, arguing that the path given by GBCD $\rho(\alpha,t)$ is the one most likely to occur and the minimizing path has the highest probability, the minimum principle was derived in [7–11, 13] for the GBCD:

$$\frac{\mu}{2\tau}d(\rho,\rho^*)^2 + F_\sigma(\rho) = \inf_{\{\eta\}}\left\{\frac{\mu}{2\tau}d(\eta,\rho^*)^2 + F_\sigma(\eta)\right\}, \tag{26}$$

where $\rho^* = \rho(\cdot,t_0)$ and $\rho = \rho(\cdot,t_0+\tau)$. This suggests an implicit scheme. Thus, for each relaxation time $\tau>0$ we determine iteratively the sequence $\{\rho^{(k)}\}$ by choosing $\rho^* = \rho^{(k-1)}$ and $\rho^{(k)} = \rho$ in (26) and set

$$\rho^{(\tau)}(\alpha,t) = \rho^{(k)}(\alpha) \quad \text{in } \Omega \text{ for } (k-1)\tau < t \leqq k\tau. \tag{27}$$

We then anticipate recovering the GBCD ρ as

$$\rho(\alpha,t) = \lim_{\tau\to 0}\rho^{(\tau)}(\alpha,t), \tag{28}$$

with the limit taken in a suitable sense. The ρ obtained from (28) is the solution of the Fokker–Planck Equation (FP), [18],

$$\mu\frac{\partial\rho}{\partial t} = \frac{\partial}{\partial\alpha}\left(\sigma\frac{\partial\rho}{\partial\alpha} + \psi'\rho\right) \quad \text{in } \Omega,\ 0<t<\infty. \tag{29}$$

The extent to which the harvested GBCD satisfied (26) will be a consequence of our gradient flow validation. We might point out here, as well, that a solution of (29) with periodic boundary conditions and nonnegative initial data is positive for $t>0$. For the detailed derivation of the FP model (29) for the GBCD obtained from the 1D simplified model of a grain boundary network, see [7–11, 13]. Analogous considerations hold for the 2D network, cf. [21].

4. The gradient flow formulation

The De Giorgi ideas about gradient flows, [4], have proven especially fruitful in studying the structure of flows on metric spaces. They can naturally exhibit the optimal mass transport basis of the flow. The GBCD, unlike this situation as it

is presented to us, is a discrete sample of an unknown process, albeit with the hypothesized theory just presented. We shall seek to adapt the gradient flow method to validate our theory. We begin with a brief review. Consider a smooth family of probability densities $\rho = \rho(x,t)$ in $\Omega \subset \mathbb{R}$, an interval. De Giorgi's observation is that

$$\frac{d}{dt}F_\sigma(\rho) = \int_\Omega \left(\sigma\frac{\rho_x}{\rho} + \psi'\right) v\rho\, dx \geqq -\frac{1}{2}\int_\Omega \left(\sigma\frac{\rho_x}{\rho} + \psi'\right)^2 \rho\, dx - \frac{1}{2}\int_\Omega v^2\rho\, dx, \tag{30}$$

where (v,ρ) satisfies satisfy the continuity equation

$$\rho_t + (v\rho)_x = 0, \quad \text{in } \Omega,\ t > 0, \tag{31}$$

with equality in (30) only if the two integrands on the right hand side are proportional. Integrating, we arrive at the dissipation inequality for F_σ. In a relaxation time interval, say $(0,\tau)$ chosen for simplicity here,

$$F_\sigma(\rho)|_{t=0} - \left\{F_\sigma(\rho)|_{t=\tau} + \frac{1}{2}\int_0^\tau \int_\Omega \left(\sigma\frac{\rho_x}{\rho} + \psi'\right)^2 \rho\, dx\, dt + \frac{1}{2}\int_0^\tau \int_\Omega v^2\rho\, dx\, dt\right\} \geqq 0, \tag{32}$$

with equality if and only if

$$\rho_t = (\sigma\rho_x + \psi'\rho)_x \quad \text{or} \quad v = -\left(\sigma\frac{\rho_x}{\rho} + \psi'\right) \quad \text{in } \Omega,\ t > 0 \tag{33}$$

in (31). To summarize, (32) holds for any path $\rho = \rho(x,t)$. The path of densities $\rho = \rho(x,t)$ satisfies

$$F_\sigma(\rho)|_{t_0} - \left\{F_\sigma(\rho)|_{t_0+\tau} + \frac{1}{2}\int_{t_0}^{t_0+\tau} \int_\Omega \left(\sigma\frac{\rho_x}{\rho} + \psi'\right)^2 \rho\, dx\, dt + \frac{1}{2}\int_{t_0}^{t_0+\tau} \int_\Omega v^2\rho\, dx\, dt\right\} = 0, \quad t_0,\ \tau \geqq 0, \tag{34}$$

$$\rho_t + (v\rho)_x = 0,$$

if and only if it is a solution of (29).

To apply these ideas in the context of the discrete sampling of a process, we shall exploit the implicit scheme (26), (27). The weak Euler Equation for this problem, eg. (40) in [18], (8.4) in [27], may be written with a little manipulation

$$\frac{1}{\tau}(x - \phi(x)) + \left(\sigma\frac{\rho_x}{\rho} + \psi'\right) = 0 \quad \text{in } \Omega, \tag{35}$$

where ϕ is the transfer function from ρ to ρ^*. This means that, at the level of the implicit scheme, equality holds in (30). However the subsequent integral formulas and the notion of dissipation are not meaningful. We can correct this, at least in part, by suggesting a path from $\rho^* = \rho^{(k-1)}$ to $\rho = \rho^{(k)}$. Let us choose the geodesic path, given by the transfer function ϕ above, so with

$$\phi(x,t) = x + \frac{(\tau - t)}{\tau}(\phi(x) - x) \quad \text{in } \Omega,\ 0 < t \leqq \tau, \tag{36}$$

$$\tilde{\rho}(x,t) = (\phi_\sharp \rho)(x,t), \text{ which means}$$

$$\int_\Omega \zeta \tilde{\rho}\, dx = \int_\Omega \zeta(\phi(\xi,t))\rho(\xi)\, d\xi$$

It has the property that

$$d(\rho^*, \tilde{\rho}(\cdot,t)) = \frac{t}{\tau} d(\rho^*, \rho).$$

For this choice of path

$$v = \frac{1}{\tau}(x - \phi(x)) \quad \text{in } \Omega,\ t = \tau, \tag{37}$$

and (30) holds at $t = \tau$ and so we adopt it as our approximation to (32). In fact, as we note below, it holds with accuracy to machine zero in simulations. Finally, note that

$$\frac{1}{\tau} d(\rho, \rho^*)^2 = \int_0^\tau \int_\Omega \left(\frac{1}{\tau}(x - \phi(x))\right)^2 \rho\, dx\, dt = \frac{1}{\tau} \int_\Omega (x - \phi(x))^2 \rho\, dx \tag{38}$$

which leads to the approximation formula

$$F_\sigma(\rho)|_{t_0} - \left\{ F_\sigma(\rho)|_{t_0+\tau} + \frac{1}{\tau} d(\rho(\cdot,t_0), \rho(\cdot,t_0+\tau))^2 \right\} \approx 0, \quad t_0,\ \tau \geqq 0. \tag{39}$$

Similarly, we can formulate a condition in terms of the dissipation. This is

$$F_\sigma(\rho)|_{t_0} - \left\{ F_\sigma(\rho)|_{t_0+\tau} + \tau \int_\Omega \left(\sigma \frac{\rho_x}{\rho} + \psi'\right)^2 \rho\, dx|_{t_0+\tau} \right\} \approx 0, \quad t_0,\ \tau \geqq 0. \tag{40}$$

We present the results below based on (39) although we computed both (39) and (40) and these results coincide.

5. Validation tests

We now begin the validation step of the Fokker–Planck model for GBCD evolution. There is an as yet unknown temperature-like parameter σ in the free energy F_σ that we determine first.

5.1. Relative entropy test

Here as the first step of validation, we review and apply the relative entropy validation procedure developed originally in [7–11, 13]. To estimate the parameter σ we look for the stationary solution of the Fokker–Planck equation (29), which is given by the Boltzmann distribution denoted as:

$$\rho_\sigma(\alpha) = \frac{1}{Z_\sigma} e^{-\frac{\psi(\alpha)}{\sigma}}, \tag{41}$$

with partition function, i.e., normalization factor

$$Z_\sigma = \int_\Omega e^{-\frac{\psi(\alpha)}{\sigma}} d\alpha.$$

Also, recall that solutions of the Fokker–Planck equation (29) have the property that they converge exponentially fast to ρ_σ in Kullback–Leibler (KL) relative entropy. KL relative entropy or KL divergence, is a particular f-divergence, i.e. it is a particular function that measures the difference between two probability densities (see e.g. [14, 15]). Let $\Phi(\rho\|\rho_\lambda)$ denote the Kullback–Leibler relative entropy (KL relative entropy) between a probability density ρ and ρ_λ, the Boltzmann distribution with parameter λ,

$$\begin{aligned} \Phi(\rho\|\rho_\lambda) &= \int_\Omega \rho \log \frac{\rho}{\rho_\lambda} d\alpha \\ &= \frac{1}{\lambda} F_\lambda + \log Z_\lambda \\ &= \frac{1}{\lambda}(F_\lambda(\rho) - F_\lambda(\rho_\lambda)) \end{aligned} \tag{42}$$

We know that if the GBCD $\rho(\alpha, t)$ evolves according to (29), it must converge exponentially fast to $\rho_\sigma(\alpha)$ in KL relative entropy as $t \to \infty$. In other words, the free energy of the grain boundary system must decrease (exponentially fast) to the free energy of the Boltzmann distribution $\rho_\sigma(\alpha)$. This concept was introduced originally in [7–11, 13] to estimate σ as described in the next paragraph.

Consider the final time T_∞ of the harvested GBCD $\rho(\alpha, T_\infty)$. Typically $T_\infty = T(80\%)$ is the simulation time when 80% of the initial grain boundaries have been removed. This time corresponds to the stationary configuration in 2D simulation in the sense that the configuration is essentially stagnant. Assuming $\rho(\alpha, T_\infty)$ as the steady-state of the GBCD, the parameter σ can be estimated via

$$\sigma = \operatorname*{argmin}_{\lambda>0} \Phi(\rho(\cdot, T_\infty)\|\rho_\lambda). \tag{43}$$

With

$$\psi_\lambda = \frac{\psi}{\lambda} + \log Z_\lambda, \tag{44}$$

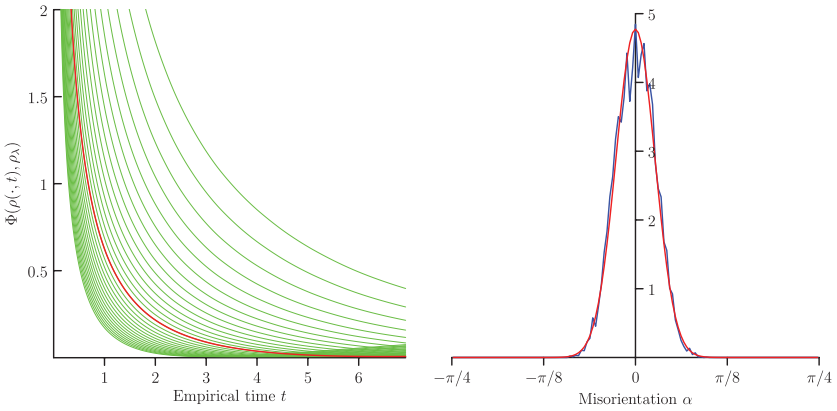

Figure 5. Single 1D trial with 2^{15} initial grain boundaries: (a) Relative entropy curves $\Phi_\lambda(\rho(\cdot,t))$ for 30 uniformly spaced trial values $\lambda \in [0.01, 0.05]$. The red curve depicts the optimal curve for $\sigma \approx 0.027931$. (b) Comparison of the steady-state empirical GBCD (80% removal) and the exact Boltzmann distribution ρ_σ for the obtained $\sigma \approx 0.027931$.

this minimization is a convex duality type of optimization problem, namely, to find the σ for which

$$\int_\Omega \{\psi_\sigma \rho + \rho \log \rho\}\, d\alpha = \inf_{\{\psi_\lambda\}} \int_\Omega \{\psi_\lambda \rho + \rho \log \rho\}\, d\alpha, \tag{45}$$

recognizable as a maximum likelihood estimate. The above procedure finds the unique value of λ for which the free energies $F_\lambda(\rho(\cdot, T_\infty))$ and $F_\lambda(\rho_\lambda)$ best agree, which is also the value of λ for which the Boltzmann distribution $\rho_\lambda(\alpha)$ best matches $\rho(\alpha, T_\infty)$.

We summarize this idea numerically in Fig. 5–6 ($n = 2^{15}$ initial grain boundaries) and in Fig. 10–11 ($n = 2^{18}$ initial grain boundaries) for the 1D system and in Fig. 15–16 ($n = 10000$ initial number of grains) and in Fig. 19–20 ($n = 20000$ initial number of grains) for the 2D system, and reader can consult [7–11, 13] for the original formulation of this validation procedure. From the relative entropy test illustrated in Fig. 5–6 and in Fig. 10–11 (for the 1D model of coarsening) and in Fig. 15–16 and in Fig. 19–20 (for the 2D model of coarsening), cf. Fig. 3, we clearly see very good agreement between the Boltzmann distribution, the steady-state solution of the Fokker–Planck equation (29), and the steady-state GBCD for both 1D and 2D models. One can also observe that the 1D model and 2D large scale computational model capture the important aspects of the GBCD evolution as illustrated in the corresponding tests in Figs. 7, 12, 17 and 21. In these tests we compare the GBCD and the solution of the Fokker–Planck equation (29) at different instants in time (where we have selected the Fokker–Planck time scaling for GBCD, see Section 5.2, and the diffusion coefficient σ in (29) is obtained from the corresponding relative entropy tests discussed above).

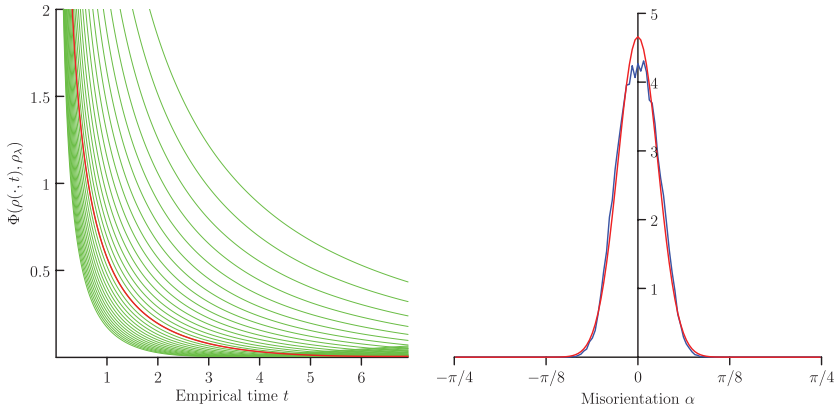

Figure 6. Average over 10 1D trials with 2^{15} initial grain boundaries: (a) Relative entropy curves $\Phi_\lambda(\rho(\cdot,t))$ for 30 uniformly spaced trial values $\lambda \in [0.01, 0.05]$. The red curve depicts the optimal curve for $\sigma \approx 0.02931$. (b) Comparison of the steady-state GBCD (80% removal) and the exact Boltzmann distribution ρ_σ for the obtained $\sigma \approx 0.02931$.

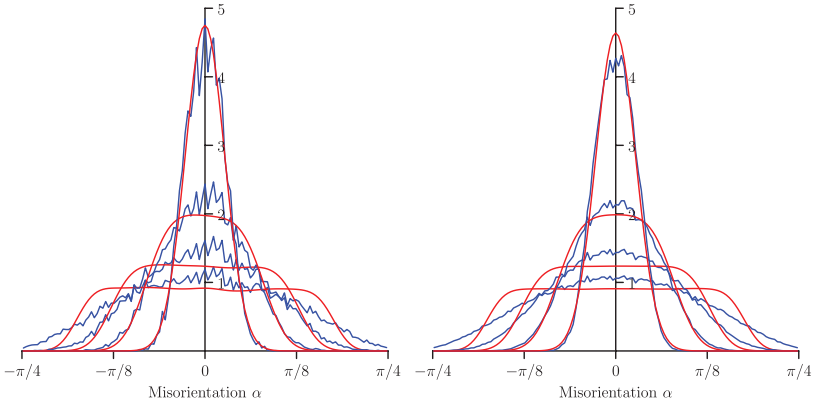

Figure 7. Single 1D trial with 2^{15} initial grain boundaries (left figure) and average over 10 1D trials with 2^{15} initial grain boundaries (right figure): Comparison of the GBCD (blue) with the Fokker–Planck solution (29) (red) at times corresponding to 20%, 40%, 60% and 80% removal of the initial grain boundaries.

The observed close agreement between the empirical GBCD and the Fokker–Planck solution further validates the developed theory.

5.2. *Gradient flow and dissipation mechanisms*

We now use the dissipation estimate (39), as the next validation test of the evolution of the GBCD as the solution solution of the Fokker–Planck Equation (29). The main idea in this test is that if a density evolves according to the Fokker–

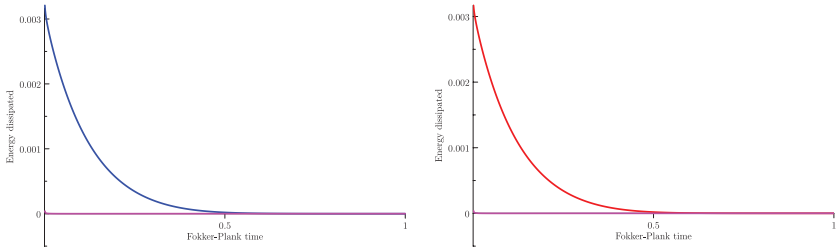

Figure 8. Fokker–Planck dissipation: The energy dissipation $F_\sigma(\rho_j^{FP}) - F_\sigma(\rho_{j+1}^{FP})$ for the solution $\rho^{FP}(\alpha, t)$ of the Fokker–Planck equation (29) (left) and the W2 distances $d(\rho_j^{\mathrm{FP}}, \rho_{j+1}^{\mathrm{FP}})^2/\tau_j$ (right) for the solution $\rho^{FP}(\alpha, t)$ of the Fokker–Planck equation (29). The time step is $\tau_j = t_{j+1} - t_j$. The difference between the energy dissipation and the squared W2 distances is depicted in magenta and indicates that the approximate dissipation identity (39) is satisfied.

Planck equation (29), it must dissipate energy according to (39). However, to employ (39), we need to select the correct time scaling for the empirical GBCD. We select the time scaling that corresponds to that of the solution of the Fokker–Planck equation. For that, we first derive a formula for an appropriate time dependent moment of the computed solution of the Fokker–Planck Equation. Inverting this formula for the time variable t (or approximately inverting it) we obtain a formula to recover time values from the density's expected values. Next, this is matched to the appropriate time dependent moment of the j^{th} profile of the empirical GBCD $\rho(\alpha, t)$, and we apply the derived formula to estimate the time parameter $t = t_j$ in $\rho(\alpha, t)$. After the time scale is set in this manner, we can proceed with verifying dissipation equality (39) for the empirical GBCD. For the detailed derivation see [6].

In the sequel, we shall use generally the abbreviation

$$\rho_j = \rho(\alpha, t_j) \tag{46}$$

and similarly for other functions.

We begin by first illustrating dissipation equality (39) for the solution of the Fokker–Planck equation, Fig. 8. We construct a numerical solution $\rho^{FP}(\alpha, t)$ of (29) with $\mu \equiv 1, \sigma = 0.02931$ and energy density function $\psi = 1 + 2\alpha^2$. We consider initial data for the GBCD as the initial condition for (29). To solve (29) numerically, we use second order finite differences for the spatial derivatives combined with Backward Euler for the time discretization. Next, for this solution $\rho^{FP}(\alpha, t)$, we compute the energy dissipation

$$F_\sigma(\rho_j^{FP}) - F_\sigma(\rho_{j+1}^{FP})$$

(left plot on Fig. 8) and the squared Wasserstein (W2) distances

$$\frac{1}{\tau_j} d(\rho_j^{\mathrm{FP}}, \rho_{j+1}^{\mathrm{FP}})^2, \quad \tau_j = t_{j+1} - t_j$$

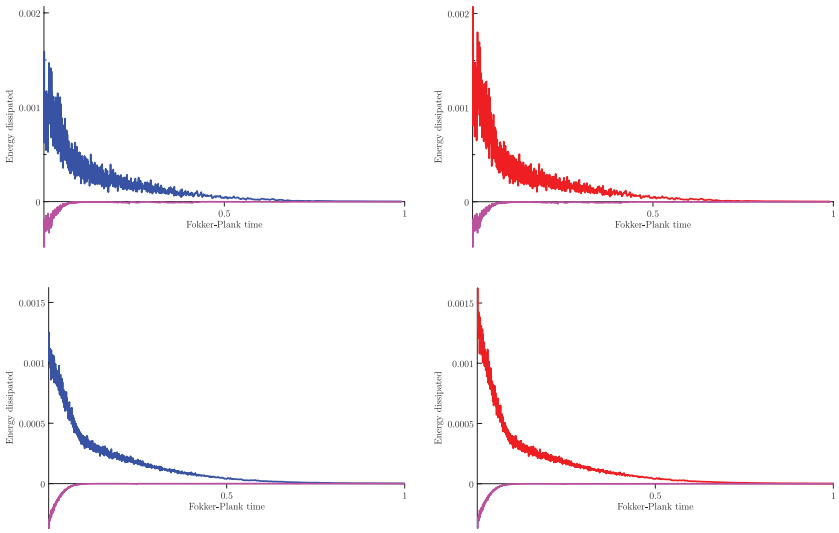

Figure 9. Single 1D trial with 2^{15} initial grain boundaries (top figure) and average over 10 1D trials with 2^{15} initial grain boundaries (bottom figure): The energy dissipation $F_\sigma(\rho_j) - F_\sigma(\rho_{j+1})$ for the GBCD (left) and the squared W2 distances $d(\rho_j, \rho_{j+1})^2/\tau_j$ (right) for the GBCD. The time step is $\tau_j = t_{j+1} - t_j$. The difference between the energy dissipation and squared W2 distances is depicted in magenta and indicates that the approximate dissipation identity (39) is satisfied.

(right plot on Fig. 8). Representative dissipation integrals were compared using (40) but are not shown. To compute squared W2 distances we employ a numerical algorithm developed in [22]. As expected, we clearly see that the dissipation equality (39) is satisfied up to machine precision for the solution of (29).

Next, we consider a time scaled GBCD harvested from the 1D critical event model, and apply the same test (39). We first apply the test to a GBCD harvested from the 1D simulation (Sec. 3) with $n = 2^{15}$ initial grain boundaries. We use $\mu \equiv 1$, the energy density $\psi = 1 + 2\alpha^2$ and harvest the GBCD at the set of empirical/numerical times. The parameter $\sigma \approx 0.02931$ is estimated using the relative entropy test of Sec. 5.1. Next, we employ time-scaling procedure for GBCD as described above to estimate the sequence of physical times $\{t_j\}_{j=1}^N$. Finally, for the GBCD $\rho(\alpha, t)$, we compute the energy dissipation

$$F_\sigma(\rho_j) - F_\sigma(\rho_{j+1})$$

(left plot on Fig. 9) and the squared W2 distances

$$\frac{1}{\tau_j} d(\rho_j, \rho_{j+1})^2, \quad \tau_j = t_{j+1} - t_j$$

(right plot on Fig. 9). We compare the energy dissipation and the squared W2 distances in Figure 9, where we see approximate agreement between the curves, away from initial times. There is some disagreement between the free energy dissipation and squared W2 distances curves at the initial time and can be explained by the finite size effect of the 1D model (i.e. grain boundaries with misorientation parameters α near the boundary of $\Omega = [-\pi/4, \pi/4]$ are not eliminated as rapidly as in later times of the simulation). Because the solution of (29) must satisfy the dissipation estimate (39), we have further validation that the Fokker–Planck equation characterizes the GBCD evolution.

In Fig. 13, we present the dissipation estimate for GBCD harvested from simulations having $n = 2^{18}$ initial grain boundaries. We observe as the number of initial grain boundaries increases (we also considered systems with $n = 2^{16}$ and $n = 2^{17}$), the dissipation estimate (39) improves. This improvement suggests that the Fokker–Planck equation is a more accurate description of GBCD evolution in a many particle limit.

Similarly, we execute the validation test (39) for the 2D model. The σ values used for validation test (39) were again estimated using the relative entropy test discussed above and are reported on the appropriate figure captions. Approximately, $\sigma = 0.16$. Again we obtain very good agreement between the energy dissipation and the squared W2 distances, see Fig. 18 (system with $n = 10000$ grains) and see Fig. 22 (system with $n = 20000$ grains). We also note that the 2D model gives better agreement between the free energy dissipation and squared W2 distances curves compared to the 1D model (the difference between the free energy dissipation curve and squared W2 distance curve that was seen for 1D model at the initial times almost disappeared for the 2D model). This validates further our theory that GBCD evolves as the solution of the Fokker–Planck equation (29).

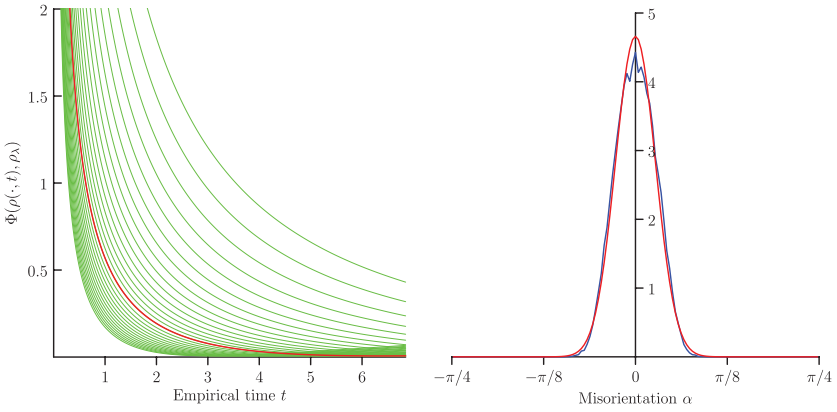

Figure 10. Single 1D trial 2^{18} initial grain boundaries: (a) Relative entropy curves $\Phi_\lambda(\rho(\cdot,t))$ for 30 uniformly spaced trial values $\lambda \in [0.01, 0.05]$. The red curve depicts the optimal curve for $\sigma \approx 0.02931$. (b) Comparison of the steady-state GBCD (80% removal) and the exact Boltzmann distribution ρ_σ for the obtained $\sigma \approx 0.02931$.

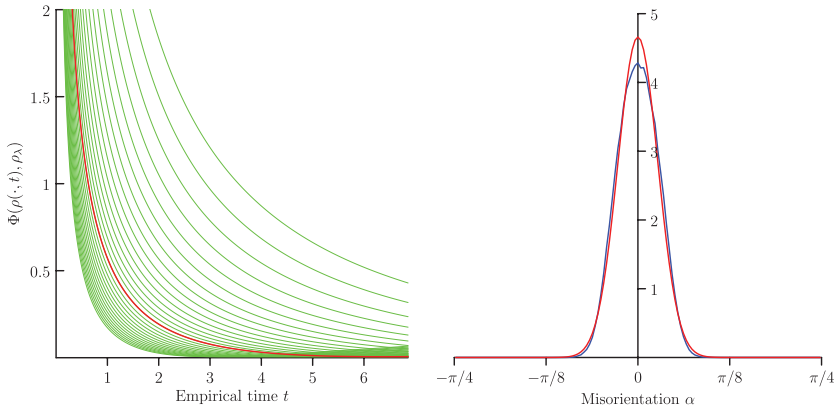

Figure 11. Average over 10 1D trials with 2^{18} initial grain boundaries: (a) Relative entropy curves $\Phi_\lambda(\rho(\cdot,t))$ for 30 uniformly spaced trial values $\lambda \in [0.01, 0.05]$. The red curve depicts the optimal curve for $\sigma \approx 0.02931$. (b) Comparison of the steady-state GBCD (80% removal) and the optimal Boltzmann distribution ρ_σ.

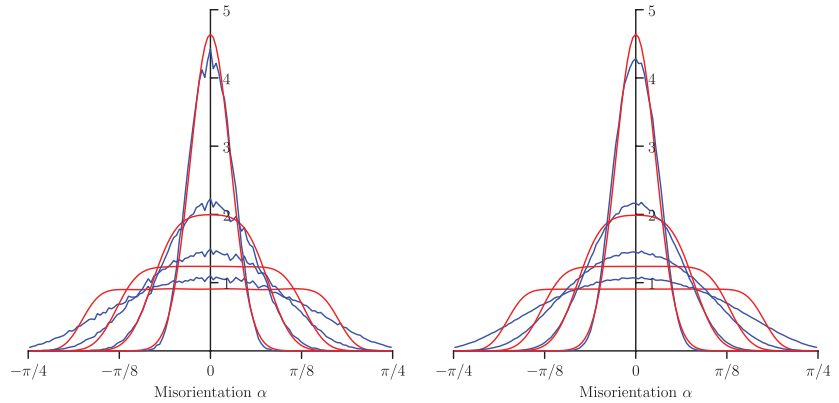

Figure 12. Single 1D trial with 2^{18} initial grain boundaries (left figure) and average over 10 1D trials with 2^{18} initial grain boundaries (right figure): Comparison of the GBCD (blue) with the Fokker–Planck solution (29) (red) at times corresponding to 20%, 40%, 60% and 80% removal of the initial grain boundaries.

5.3. Statistical validation of Fokker–Planck dynamics

We now quantify the agreement between the GBCD evolution and Fokker–Planck dynamics by asking how well (39) is satisfied in the statistical sense. Since the grain boundary system is initialized randomly, the GBCD itself is random. Thus the free energy dissipation $F_\sigma(\rho_j) - F_\sigma(\rho_{j+1})$ and the squared W2 distances $d(\rho_j, \rho_{j+1})^2$ between any two times, are themselves random variables. Therefore, we consider generating many realizations of the grain boundary system and associated statistics to determine if the energy dissipation samples and the squared

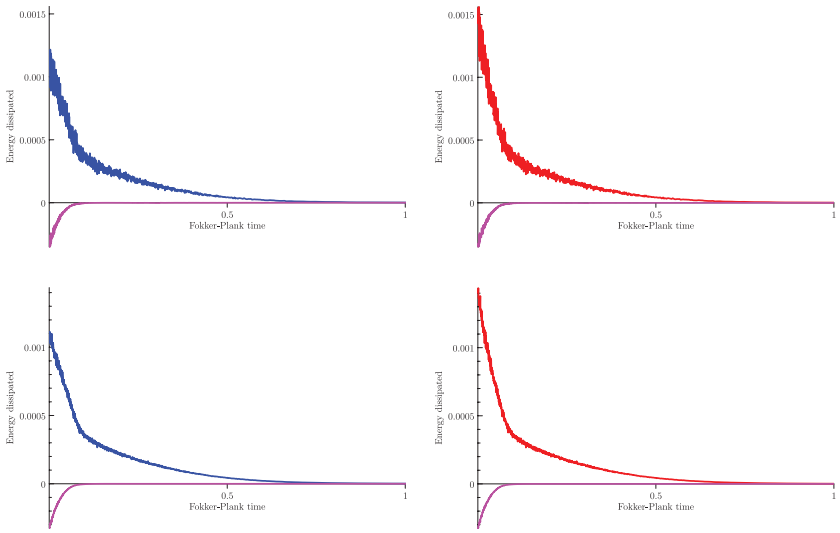

Figure 13. Single 1D trial with 2^{18} initial grain boundaries (top figure) and average over 10 1D trials with 2^{18} initial grain boundaries (bottom figure): The energy dissipation $F_\sigma(\rho_j) - F_\sigma(\rho_{j+1})$ for the GBCD (left) and the W2 distances $d(\rho_j, \rho_{j+1})^2/\tau_j$ (right) for the GBCD. The time step is $\tau_j = t_{j+1} - t_j$. The difference between the energy dissipation and squared W2 distances is depicted in magenta and indicates that the approximate dissipation identity (39) is satisfied.

W2 distance samples agree in a statistical sense. For that, we collect energy differences $\Delta F := F_\sigma(\rho_j) - F_\sigma(\rho_{j+1})$ and squared W2 distances $W2 = d(\rho_j, \rho_{j+1})^2$ at each realization of the system. Next, using these data collected from all the realizations, we define and compute the density estimators denoted as $f_{\Delta F}(e,t)$, $(e := \Delta F)$ and $f_W(e,t)$, $(e := W2)$ as the normalized histograms of the free energy differences and squared W2 distances respectively. In Fig. 14 we display the density estimators $f_{\Delta F}(e,t)$ and $f_W(e,t)$ computed for 1D system with different numbers of the initial grain boundaries $n = 2^{15}, 2^{16}, 2^{17}$ and 2^{18}. Each estimator is generated from $R = 1000$ independent realizations of the 1D coarsening system with the given number n of the initial grain boundaries. We observe from the obtained results, see Fig. 14, that the energy samples for the free energy dissipation and W2 distances appear to converge in distribution, as the number of initial grain boundaries n increases, i.e. in a many particles limit. Let us also note that at this point we were able to conduct this test only for the 1D model of the grain boundaries network due to large computational complexity of the statistical validation test for the 2D model.

6. Remarks

We are fortunate that for the simple potentials we treat here for interfacial energies, roughly speaking, quadratic and consequently related to an Ornstein–

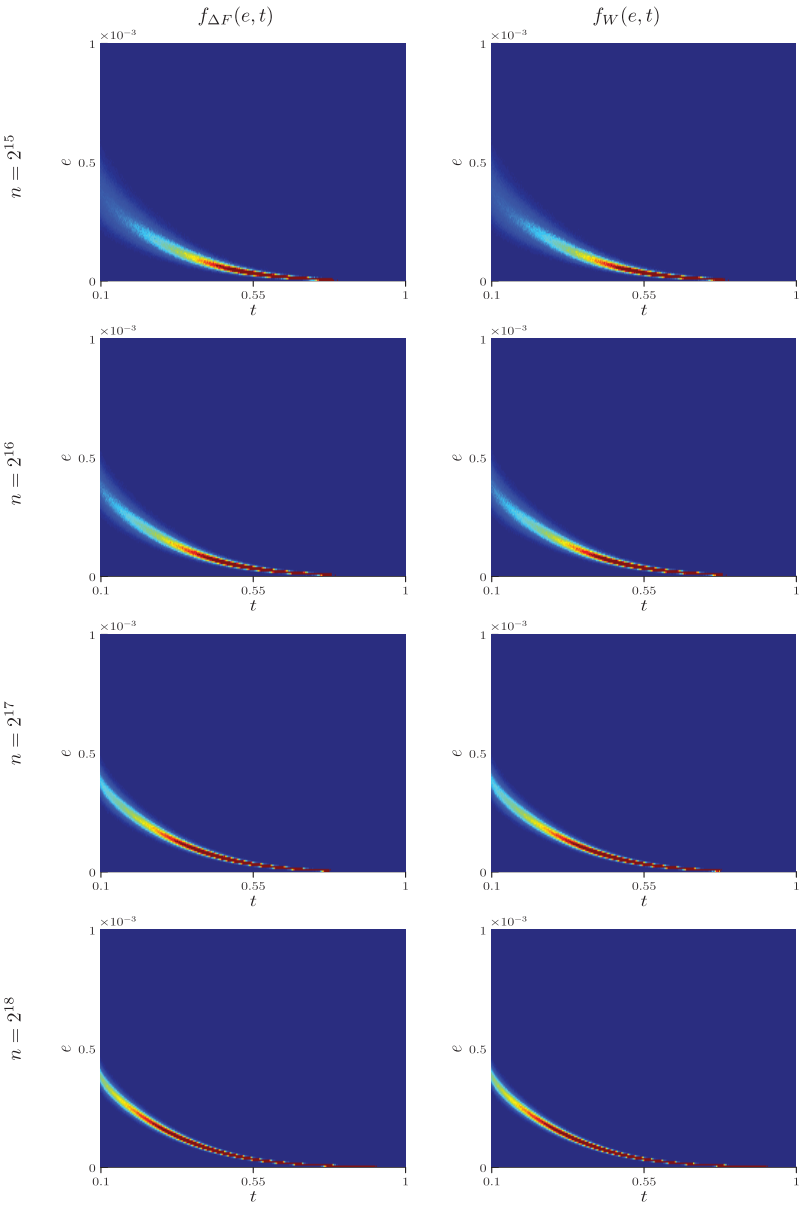

Figure 14. Density estimators (left) $f_{\Delta F}(e,t)$ for the free energy differences and (right) $f_W(e,t)$ for the squared W2 distances, and e denotes either the value of the free energy differences or W2 differences in the density estimators. The estimator $f_{\Delta F}$ (resp. f_W) is computed by appropriately normalizing a two-dimensional histogram of the free energy differences (resp. squared W2 distances) collected from $R = 1000$ realizations of the 1D coarsening simulation with $n = 2^x$ initial grain boundaries (indicated).

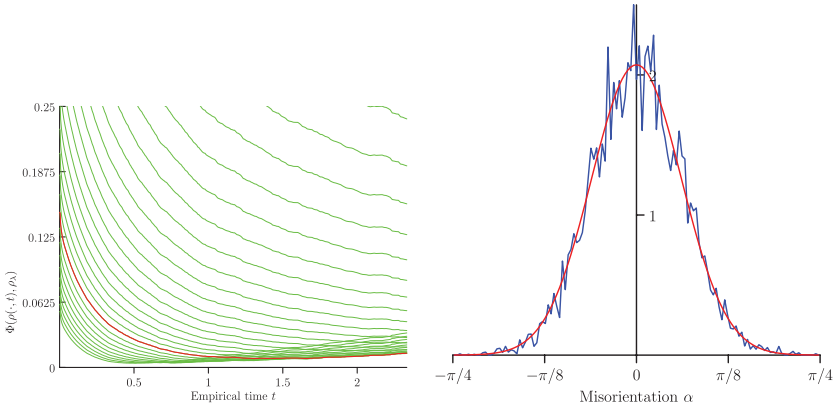

Figure 15. Single 2D trial 10000 initial grain boundaries: (a) Relative entropy curves $\Phi_\lambda(\rho(\cdot,t))$ for 30 uniformly spaced trial values $\lambda \in [0.05, 0.2]$. The red curve depicts the optimal curve for $\sigma \approx 0.148276$. (b) Comparison of the steady-state GBCD (80% removal) and the exact Boltzmann distribution ρ_σ for the obtained $\sigma \approx 0.148276$.

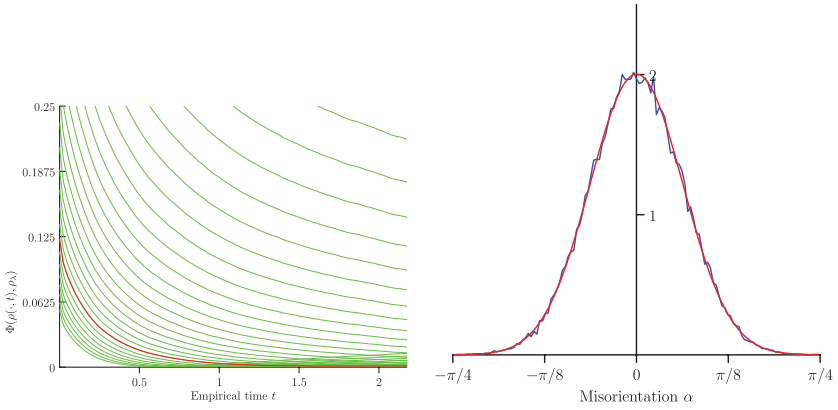

Figure 16. Average over 10 2D trials with 10000 initial grain boundaries: (a) Relative entropy curves $\Phi_\lambda(\rho(\cdot,t))$ for 30 uniformly spaced trial values $\lambda \in [0.05, 0.2]$. The red curve depicts the optimal curve for $\sigma \approx 0.158621$. (b) Comparison of the steady-state GBCD (80% removal) and the exact Boltzmann distribution ρ_σ for the obtained $\sigma \approx 0.158621$.

Uhlenbeck process, our Fokker–Planck equation is quite direct. Regardless of the potential, given that it is smooth, we find a Boltzmann stationary distribution, but the evolution need not be so simple. This is a direction to pursue. In addition, there is the challenge of extending the framework to three dimensions. Many special computational features available for the simulation of curves fail for surfaces.

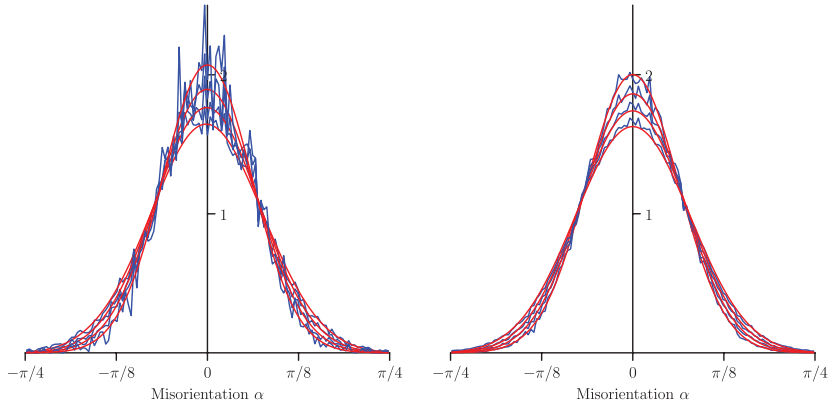

Figure 17. Single 2D trial 10000 initial grain boundaries (left figure) and average over 10 2D trials with 10000 initial grain boundaries (right figure): Comparison of the GBCD (blue) with the Fokker–Planck solution (29) (red) at times corresponding to 20%, 40%, 60% and 80% removal of the initial grain boundaries.

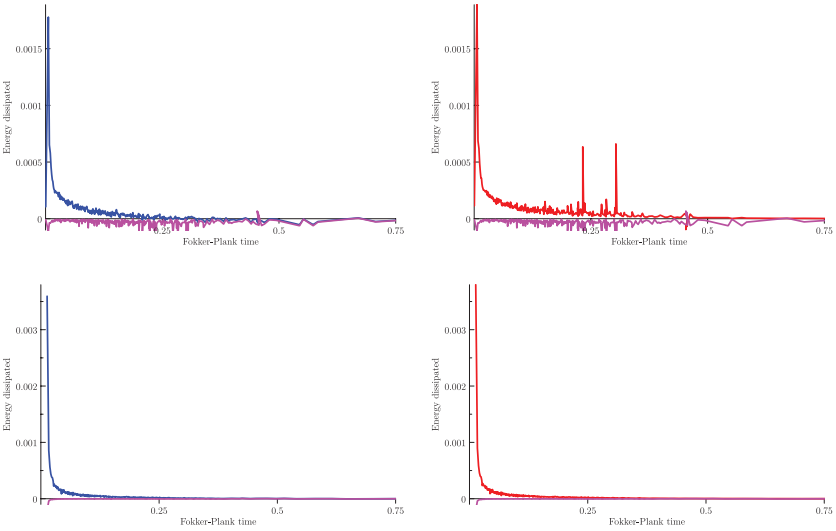

Figure 18. Single 2D trial with 10000 initial grain boundaries (top figure) and average over 10 2D trials with 10000 initial grain boundaries (bottom figure): The energy dissipation $F_\sigma(\rho_j) - F_\sigma(\rho_{j+1})$ for the GBCD (left) and the W2 distances $\frac{1}{\tau_j} d(\rho_j, \rho_{j+1})^2$ (right) for the GBCD. The time step is $\tau_j = t_{j+1} - t_j$. The difference between the energy dissipation and W2 distances is depicted in magenta and indicates that the approximate dissipation identity (39) is satisfied.

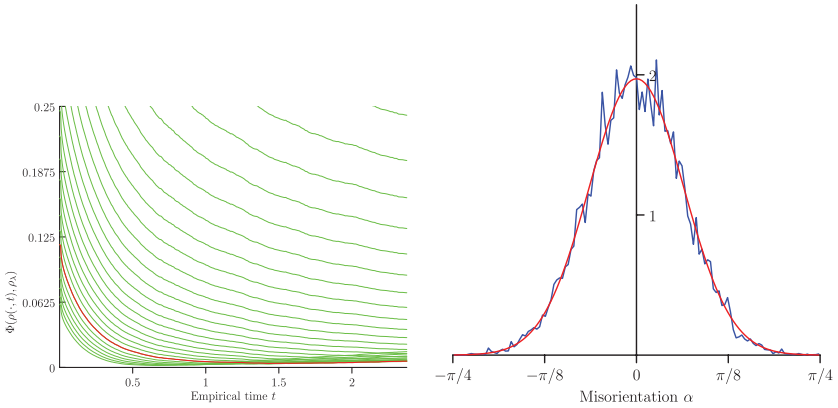

Figure 19. Single 2D trial 20000 initial grain boundaries: (a) Relative entropy curves $\Phi_\lambda(\rho(\cdot,t))$ for 30 uniformly spaced trial values $\lambda \in [0.05, 0.2]$. The red curve depicts the optimal curve for $\sigma \approx 0.163793$. (b) Comparison of the steady-state GBCD (80% removal) and the exact Boltzmann distribution ρ_σ for the obtained $\sigma \approx 0.163793$.

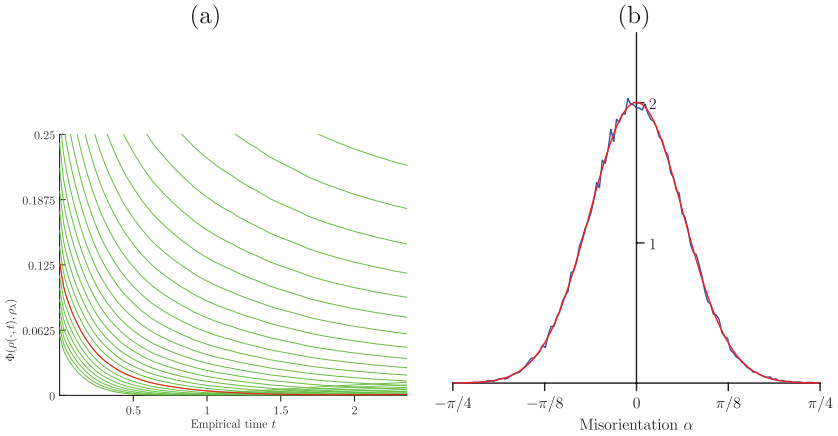

Figure 20. Average over 10 2D trials with 20000 initial grain boundaries: (a) Relative entropy curves $\Phi_\lambda(\rho(\cdot,t))$ for 30 uniformly spaced trial values $\lambda \in [0.05, 0.2]$. The red curve depicts the optimal curve for $\sigma \approx 0.158621$. (b) Comparison of the steady-state GBCD (80% removal) and the exact Boltzmann distribution ρ_σ for the obtained $\sigma \approx 0.158621$.

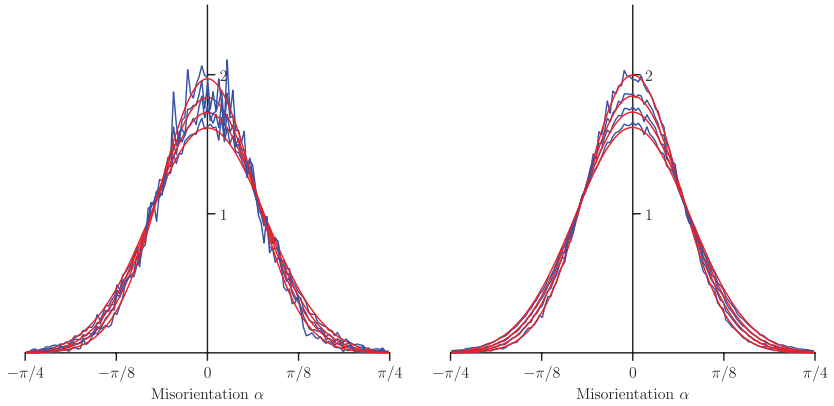

Figure 21. Single 2D trial 20000 initial grain boundaries (left figure) and average over 10 2D trials with 20000 initial grain boundaries (right figure): Comparison of the GBCD (blue) with the Fokker–Planck solution (29) (red) at times corresponding to 20%, 40%, 60% and 80% removal of the initial grain boundaries.

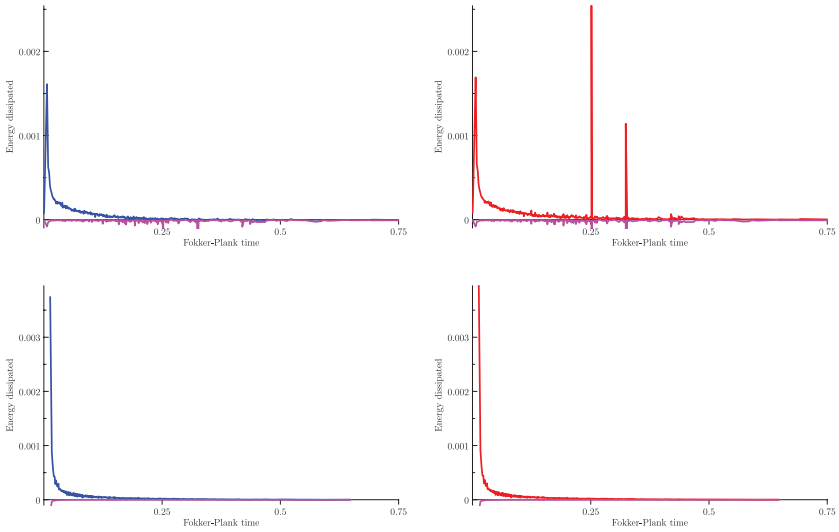

Figure 22. Single 2D trial with 20000 initial grain boundaries (top figure) and average over 10 2D trials with 20000 initial grain boundaries (bottom figure): The energy dissipation $F_\sigma(\rho_j) - F_\sigma(\rho_{j+1})$ for the GBCD (left) and the squared W2 distances $d^2(\rho_j, \rho_{j+1})/\tau_j$ (right) for the GBCD. The time step is $\tau_j = t_{j+1} - t_j$. The difference between the energy dissipation and W2 distances is depicted in magenta and indicates that the approximate dissipation identity (39) is satisfied.

ACKNOWLEDGMENTS. Research supported by NSF DMR 0520425, DMS 0405343, DMS 0305794, DMS 0806703, DMS 0635983, DMS 0915013, DMS 1112984, OISE-0967140 and Simons Foundation Grant 415673.

REFERENCES

[1] D. ABOU-RAS - N. SCHAEFER - T. RISSOM - M. N. KELLY - J. HAARSTRICH - C. RONNING - G. S. ROHRER - A. D. ROLLETT, *Grain-boundary character distribution and correlations with electrical and optoelectronic properties of CuInSe2 thin films*, Acta Materialia, 118:244–252 (2016).

[2] B. ADAMS - D. KINDERLEHRER - I. LIVSHITS - D. MASON - W. MULLINS - G. ROHRER - A. ROLLETT - D. SAYLOR - S. TA'ASAN - C. WU, *Extracting grain boundary energy from triple junction measurement*, Interface Science, 7:321–338 (1999).

[3] B. ADAMS - D. KINDERLEHRER - W. MULLINS - A. ROLLETT - S. TA'ASAN, *Extracting the relative grain boundary free energy and mobility functions from the geometry of microstructures*, Scripta Materiala, 38(4):531–536 (1998).

[4] L. AMBROSIO - N. GIGLI, *Modelling and Optimisation of Flows on Networks*, chapter A User's Guide to Optimal Transport, pages 1–155. Springer Berlin Heidelberg, Berlin, Heidelberg (2013).

[5] L. AMBROSIO - N. GIGLI - G. SAVARÉ, *Gradient flows in metric spaces and in the space of probability measures*, Lectures in Mathematics ETH Zürich. Birkhäuser Verlag, Basel, second edition (2008).

[6] P. BARDSLEY, *Intensity-only imaging with waves, restarted inverse Born series, and analysis of coarsening in polycrystalline materials*, Ph.D. thesis, The University of Utah (2016).

[7] K. BARMAK - E. EGGELING - M. EMELIANENKO - Y. EPSHTEYN - D. KINDERLEHRER - R. SHARP - S. TA'ASAN, *Predictive theory for the grain boundary character distribution*, In Proc. Recrystallization and Grain Growth IV (2012).

[8] K. BARMAK - E. EGGELING - M. EMELIANENKO - Y. EPSHTEYN - D. KINDERLEHRER - R. SHARP - S. TA'ASAN, *Critical events, entropy, and the grain boundary character distribution*, Phys. Rev. B, 83:134117 (2011).

[9] K. BARMAK - E. EGGELING - M. EMELIANENKO - Y. EPSHTEYN - D. KINDERLEHRER - R. SHARP - S. TA'ASAN, *An entropy based theory of the grain boundary character distribution*, Discrete Contin. Dyn. Syst., 30(2):427–454 (2011).

[10] K. BARMAK - E. EGGELING - M. EMELIANENKO - Y. EPSHTEYN - D. KINDERLEHRER - R. SHARP - S. TA'ASAN, *A theory and challenges for coarsening in microstructure*, In Analysis and numerics of partial differential equations, volume 4 of Springer INdAM Ser., pages 193–220. Springer, Milan (2013).

[11] K. BARMAK - E. EGGELING - M. EMELIANENKO - Y. EPSHTEYN - D. KINDERLEHRER - R. SHARP - S. TA'ASAN, *Materials microstructure: entropy and curvature driven coarsening*, In RIMS Proceedings, volume 1881, pages 71–91. Research Institute for Mathematical Sciences, U. Kyoto (2014).

[12] K. BARMAK - E. EGGELING - M. EMELIANENKO - Y. EPSHTEYN - D. KINDERLEHRER - R. SHARP - S. TA'ASAN, *Recent developments in material microstructure: a theory of coarsening*, In Symposium NN – Mathematical and Computational Aspects of Materials Science, volume 1753 of MRS Proceedings (2015).

[13] K. BARMAK - E. EGGELING - M. EMELIANENKO - Y. EPSHTEYN - D. KINDERLEHRER - S. TA'ASAN, *Geometric growth and character development in large metastable networks*, Rend. Mat. Appl. (7), 29(1):65–81 (2009).

[14] A. DasGupta, *Asymptotic Theory of Statistics and Probability*, Springer Texts in Statistics. Springer New York, New York (2008).

[15] A. Dembo - O. Zeitouni, *Large Deviations Techniques and Applications*, Stochastic Modelling and Applied Probability. Springer Berlin Heidelberg, Berlin, Heidelberg (2009).

[16] K. J. Ganesh - A. D. Darbal - S. Rajasekhara - G. S. Rohrer - K. Barmak - P. J. Ferreira, *Effect of downscaling nano-copper interconnects on the microstructure revealed by high resolution TEM-orientation-mapping*, Nanotechnology, 23(13) (2012).

[17] A. Iserles, *A first course in the numerical analysis of differential equations*, Cambridge Texts in Applied Mathematics. Cambridge University Press, Cambridge (1996).

[18] R. Jordan - D. Kinderlehrer - F. Otto, *The variational formulation of the fokker-planck equation*, SIAM J. Math. Analysis, 29(1):1–17 (1998).

[19] D. Kinderlehrer - I. Livshits - G. Rohrer - S. Ta'asan - P. Yu, *Mesoscale simulation of the evolution of the grain boundary character distribution*, Recrystallization and grain growth, pts 1 and 2, 467–470(Part 1–2):1063–1068 (2004).

[20] D. Kinderlehrer - I. Livshits - S. Ta'asan, *A variational approach to modeling and simulation of grain growth*, SIAM J. Sci. Comp., 28(5):1694–1715 (2006).

[21] D. Kinderlehrer - X. Y. Lu, *Material microstructure: Texture evolution in two dimensions*, in preparation (2016).

[22] D. Kinderlehrer - N. Walkington, *Approximation of parabolic equations using the Wasserstein metric*, Rairo-mathematical modelling and numerical analysis-modelisation mathematique et analyse numerique, 33(4):837–852 (1999).

[23] T. Laux - F. Otto, *Convergence of the thresholding scheme for multi-phase mean-curvature flow*, Calc. Var. Partial Differential Equations, 55(5):Paper No. 129, 74 (2016).

[24] W. Mullins, *2-Dimensional motion of idealized grain growth*, Journal Applied Physics, 27(8):900–904 (1956).

[25] G. Rohrer, *Influence of interface anisotropy on grain growth and coarsening*, Annual Review of Materials Research, 35:99–126 (2005).

[26] A. D. Rollett - S.-B. Lee - R. Campman - G. S. Rohrer, *Three-dimensional characterization of microstructure by electron back-scatter diffraction*, Annual Review of Materials Research, 37:627–658 (2007).

[27] F. Santambrogio, *Optimal transport for applied mathematicians*, volume 87 of Progress in Nonlinear Differential Equations and their Applications, Birkhäuser Verlag, Basel (2015).

[28] J. von Neumann, *Discussion remark concerning paper of C. S. Smith ''grain shapes and other metallurgical applications of topology''*, In Metal Interfaces, pages 108–110. American Society for Metals, Cleveland, Ohio (1952).

Received 26 January 2017,
and in revised form 6 June 2017.

Patrick Bardsley
Institute for Computational Engineering and Sciences
The University of Texas at Austin
201 E 24th Street, POB 3.342
Austin
TX 78712, USA
bardsley@ices.utexas.edu

Katayun Barmak
Department of Applied Physics and Applied Mathematics
Columbia University
500 West 120th Street
Suite 200, MC 4701
New York
NY 10027, USA
katakyn.barmak@columbia.edu

Eva Eggeling
Fraunhofer Austria Research GmbH
Visual Computing
Inffeldgasse 16c
A-8010 Graz, Austria
eva.eggeling@fraunhofer.at

Yekaterina Epshteyn
Department of Mathematics
The University of Utah
155 S 1400 E
Salt Lake City
UT 84112, USA
epshteyn@math.utah.edu

David Kinderlehrer
Department of Mathematical Sciences
Carnegie Mellon University
5000 Forbes Ave.
Pittsburgh
PA 15213, USA
davidk@cmu.edu

Shlomo Ta'asan
Department of Mathematical Sciences
Carnegie Mellon University
5000 Forbes Ave.
Pittsburgh
PA 15213, USA
shlomo@andrew.cmu.edu